Dalton Transactions

ROYAL SOCIETY OF CHEMISTRY

PAPER

View Article Online
View Journal | View Issue

Check for updates

Cite this: *Dalton Trans.*, 2023, **52**, 8135

A Pd_4L_2 cage containing Brønsted-base active sites for the one-pot photooxidation/Knoevenagel condensation reaction†

Yan-Fang Zhou,[a,b] Dan-Ni Yan,[b] Shao-Jun Hu,[b] Li-Peng Zhou,[b] Li-Xuan Cai *[a,b] and Qing-Fu Sun *[a,b]

Received 17th March 2023,
Accepted 12th May 2023

DOI: 10.1039/d3dt00815k

rsc.li/dalton

Brønsted-base active sites on a Pd_4L_2 cage facilitates enhanced catalytic efficiency, wide substrate scope and high turnover number (TON) for the one-pot photooxidation/Knoevenagel condensation reaction under mild conditions.

Open Access Article. Published on 15 May 2023. Downloaded on 8/6/2025 5:20:31 AM.
This article is licensed under a Creative Commons Attribution 3.0 Unported Licence.

Introduction

Both the microenvironment and the active sites are crucial for natural enzymes to realize highly efficient and selective catalytic transformations.[1,2] Developing equivalent artificial catalysts that can mimic enzymes' structure and function has been a long-sought goal for supramolecular chemists.[3–8] Coordination-assembled metallocages with well-defined three-dimensional (3D) cavities are attractive platforms for supramolecular catalysis.[9–22] The introduction of active sites, such as chiral,[20,23,24] photoactive,[25–27] and Lewis acid–base sites,[10] onto cage skeletons has been shown to be a promising strategy to endow the native host with catalytic functions. Moreover, integration of the active sites and the cage's confinement effect can also lead to enhanced selectivity toward conventional reactions.[28]

One-pot sequential reactions that can achieve continuous multiple chemical transformations without tedious isolation and purification of reaction intermediates are attractive in organic synthesis.[29–34] Recently, we have reported a series of pyridinium-functionalized organo-palladium cages, which can be utilized for both photooxidation[35] and Knoevenagel condensation[36] reactions. Herein, we report two Pd_4L_2-type cages (**1** and **2**) built from the same *cis*-blocking (tmen)$Pd(NO_3)_2$ (tmen = tetramethylethylenediamine) metal corners (Pd), and two bis-TPT [TPT = 2,4,6-tris(4-pyridyl)-1,3,5-triazine] ligands bridged by either a 1,3-dimethylene-pyridine (L^1) or a 1,3-dimethylene-benzene (L^2) spacer (Scheme 1). Cage **1**, decorated with Brønsted-base pyridine sites, shows enhanced catalytic efficiency toward the one-pot photooxidation/Knoevenagel condensation reaction, with a wide substrate scope, size-selectivity and high reaction turnover number (TON).

Results and discussion

Ligand design and synthesis

With the aim of introducing Brønsted base functional sites into the cavity of the hosts, ligand L^1 with a 1,3-dimethylene pyridine spacer and ligand L^2 with 1,3-dimethylene benzene as a control were designed and prepared by similar procedures. Both ligands were synthesized by heating an excess amount of

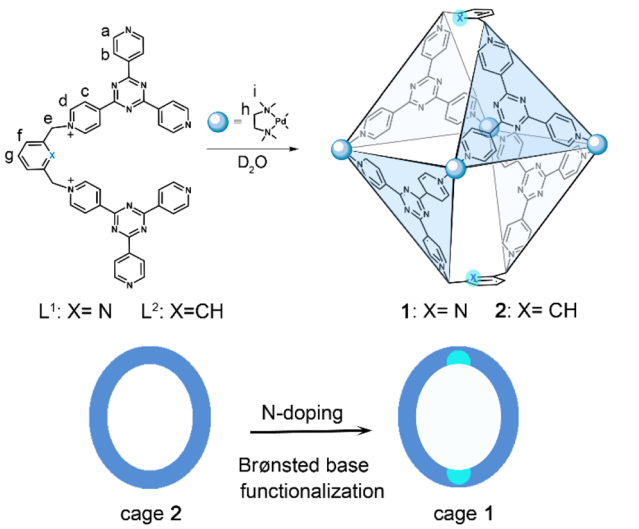

Scheme 1 Self-assembly of cages **1** ($Pd_4L^1_2$) and **2** ($Pd_4L^2_2$), highlighted with cavity modification by introduction of Brønsted-base active sites.

[a]*College of Chemistry, Fuzhou University, Fuzhou 350108, People's Republic of China. E-mail: lxcai@fjirsm.ac.cn, qfsun@fjirsm.ac.cn*
[b]*Fujian College, University of Chinese Academy of Sciences, State Key Laboratory of Structural Chemistry, Fujian Institute of Research on the Structure of Matter, Chinese Academy of Sciences, Fuzhou 350002, People's Republic of China*

†Electronic supplementary information (ESI) available. CCDC 2246529 and 2246530. For ESI and crystallographic data in CIF or other electronic format see DOI: https://doi.org/10.1039/d3dt00815k

Open Access Article. Published on 15 May 2023. Downloaded on 8/6/2025 5:20:31 AM.
This article is licensed under a Creative Commons Attribution 3.0 Unported Licence.

TPT with 1,3-bis(bromomethyl)benzene or 2,6-bis(bromomethyl)pyridine at 115 °C in DMF under a N_2 atmosphere, followed by counterion exchange of excess $NaBF_4$ (see the Experimental section for details).

Self-assembly of Pd_4L_2-type cages 1 and 2

When L^1 (8.89 μmol) was treated with (tmen)Pd$(NO_3)_2$ (16 μmol) in 4 mL of D_2O with vigorous stirring at 50 °C for 15 min, the suspension of the ligand turned into a clear light-orange solution. ^{1}H NMR spectra confirmed the quantitative formation of cage **1** with all the proton signals fully assigned based on a ^{1}H–^{1}H COSY experiment (Fig. S5–S10†). Compared to that on free L^1, the downfield-shifting of the pyridyl doublets (9.35 and 9.28 ppm for H_a, 8.76 ppm for H_b) indicated the successful coordination to Pd(II) (Fig. 1A and B). The appearance of only one set of 11 peaks in the ^{1}H NMR spectrum indicated the high symmetry of cage **1**. The diffusion-ordered spectroscopy (DOSY) NMR spectrum also suggested the formation of a single species with a diffusion coefficient of 3.20×10^{-10} m^2 s^{-1}, corresponding to a diameter of 1.53 nm (Fig. S10†). After counter-ion exchange with NH_4PF_6, ESI-TOF-MS analyses clearly confirmed the formation of the Pd_4L_2-type cages, where a series of peaks with charge states varying from 3+ to 6+ were observed due to the progressive loss of PF_6^- counterions. For example, peaks observed at m/z = 536.5657, 672.8510, 877.3541, and 1217.7918 could be assigned to $[Pd_4L^1{}_2(PF_6)_6]^{6+}$, $[Pd_4L^1{}_2(PF_6)_7]^{5+}$, $[Pd_4L^1{}_2(PF_6)_8]^{4+}$, and $[Pd_4L^1{}_2(PF_6)_9]^{3+}$ charged species, respectively. Cage **2** was also prepared quantitatively by a similar procedure as above by replacing L^1 with L^2 (Fig. 1C and D).

Structures of both L^1 and cage **2** have been confirmed by single-crystal X-ray diffraction studies. In the solid state, L^1 adopts a clip conformation with clear intramolecular π–π interaction (3.33 Å) between two TPT panels (Fig. 2A). In the crystal structure of cage **2**, two cationic pyridinium ligands are connected by four (tmen)Pd capping units, which is consistent with the Pd_4L_2 crystal structure that we have reported.[37] Four Pd(II) ions sit in the middle with the diagonal Pd–Pd distances being 19.2389(6) Å and 17.3411(6) Å (Fig. 2B). The cavity volume of cage **2** was calculated to be 834 Å^3 using the 3 V Web server,[38] which is slightly larger than the cavity of our previous Pd_4L_2 cage (Fig. S20†).[37]

Cyclic voltammetry experiments (CVs) for L^1 and cage **1** were performed to investigate their redox properties (Fig. 3). Three reversible reduction waves for L^1 were observed at around −0.402, −0.526 and −0.975 V *vs.* Ag/AgCl. The first two reduction peaks are attributed to the reduction processes on pyridinium units, to form a neutral state. The last one is assigned to two-electron reduction processes on the triazine unit. Cage **1** showed four reversible redox waves at around

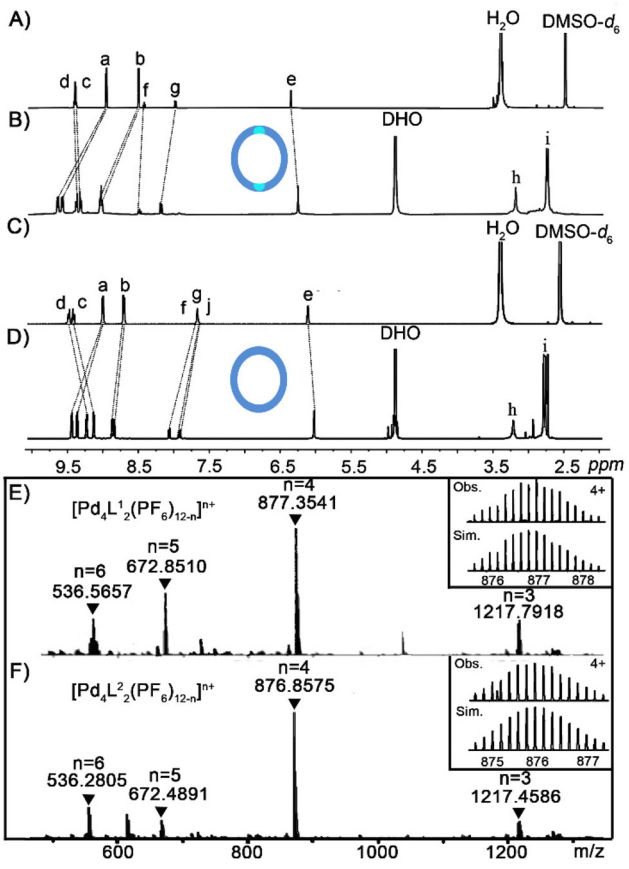

Fig. 1 (A) ^{1}H NMR spectra (400 MHz, 298 K) of L^1 in DMSO-d_6, (B) cage **1** in D_2O, (C) L^2 in DMSO-d_6 and (D) cage **2** in D_2O. ESI-TOF-MS spectra for Pd_4L_2 cages (E) **1** and (F) **2** with the inset showing the observed and simulated isotopic patterns of the 4+ peaks.

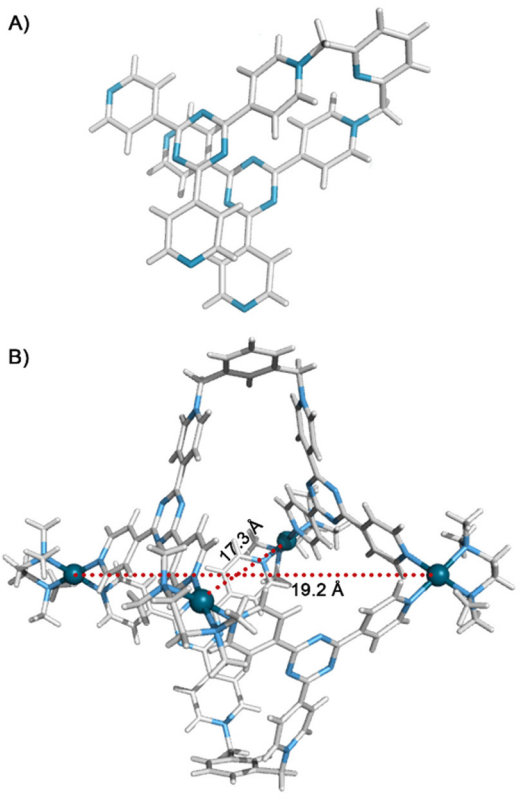

Fig. 2 X-ray structures of ligand L^1 (A) and cage **2** (B) (counterions and solvent molecules are omitted for clarity).

This journal is © The Royal Society of Chemistry 2023

Open Access Article. Published on 15 May 2023. Downloaded on 8/6/2025 5:20:31 AM.
This article is licensed under a Creative Commons Attribution 3.0 Unported Licence.

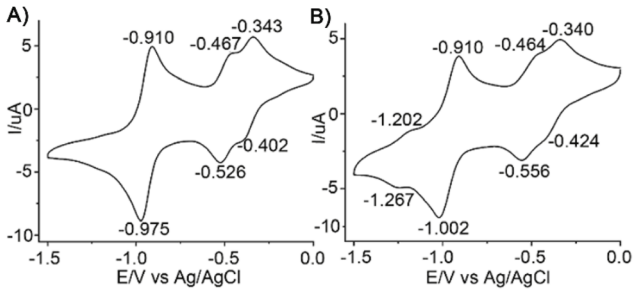

Fig. 3 Cyclic voltammograms of (A) ligand L^1 (1.0 mM) and (B) cage **1** (0.5 mM) in DMSO at a 0.1 V s^{-1} scan rate. Bu_4NPF_6 (0.1 M) was used as a supporting electrolyte.

−0.424, −0.556, −1.022 and −1.267 V. Compared with L^1, the reduction potential of cage **1** appeared at more negative positions, indicating that the cage skeleton maintains the redox properties of pyridine derivatives but becomes more difficult to be reduced due to coordination with Pd(II). Moreover, the electronic communication between ligands takes place through coordination bonds.

Photocatalytic performance of cage 1 toward a one-pot sequential reaction

The redox-active nature of cage **1** and the installation of Brønsted base active sites motivated us to further study its potential in the one-pot photooxidation/Knoevenagel condensation reaction (Fig. 4). A suspension of 4-bromophenyl methanol (**3a**, 10 equiv.) was added to a D_2O solution of **1** at room temperature. After the addition of an excess amount of malononitrile (*ca.* 20 equiv.) as the condensation reactant, the resulting solution was irradiated under purple LEDs at room temperature for 5 h. After reaction, the signals of **3a** disappeared completely and a large amount of white solid precipitated. After CH_2Cl_2 extraction, ^{1}H NMR showed that the substrate was fully consumed and a new set of signals attributable to benzylidene malononitrile (**4a**) appeared (99% yield and 100% chemoselectivity) (Table 1, entry 1, Fig. S26†). Control

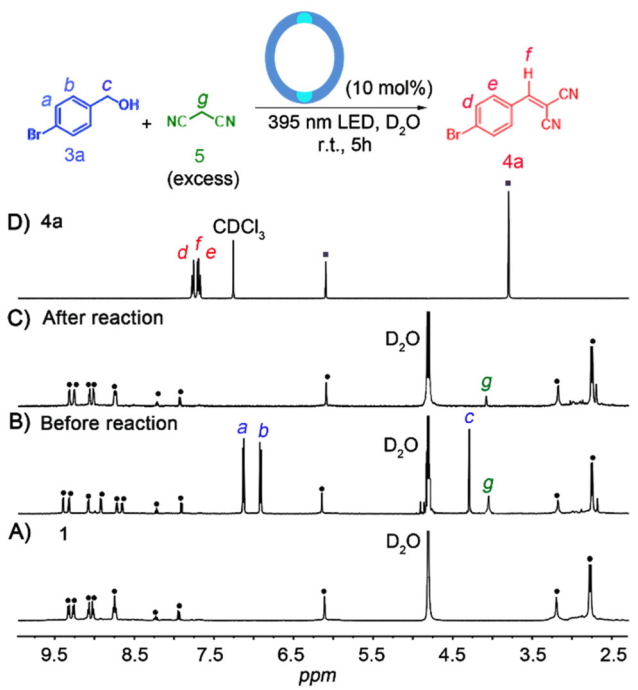

Fig. 4 One-pot photooxidation/Knoevenagel condensation of **3a** with malononitrile (**5**) catalyzed by cage **1**. ^{1}H NMR spectra (400 MHz, D_2O, 298 K) of (A) free cage **1**, (B) after addition of **3a** and **5** to cage **1**, (C) after sequential reaction, (D) crude product **4a** obtained by extraction and dissolved in $CDCl_3$ with 1,3,5-trimethoxybenzene as an internal standard (labelled by ■). The signals of cage **1** were labelled with ●.

Table 1 One-pot sequential photooxidation-Knoevenagel condensation reactions[a]

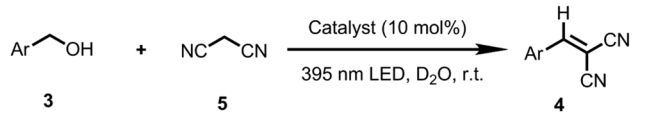

3 5 4

Entry	Substrates **3**	Time	Catalyst	Yield[b] (%)
1	**3a**	5 h	**1**	99
2[c]		5 h	**1**	27
3[d]		5 h	**1**	40
4[e]		5 h	$L^1{\cdot}2BF_4$	14
5[f]		5 h	$(tmen)Pd(NO_3)_2$	3
6[g]		5 h	**1**	n.d.
7		5 h	**2**	66
8	**3b**	10 h	**1**	61
9	**3c**	7 h	**1**	65
10	**3d**	5 h	**1**	96
11	**3e**	7 h	**1**	77
12	**3f**	7 h	**1**	97
13	**3g**	4 h	**1**	99
14	**3h**	12 h	**1**	76
15	**3i**	7 h	**1**	95
16	**3j**	5 h	**1**	99
17	**3k**	24 h	**1**	n.d.

[a] Standard reaction conditions: benzyl alcohols (0.01 mmol, 10 equiv.) and malononitrile (0.020 mmol, 20 equiv.) were added to the solution of catalysts (0.001 mmol, 1 equiv.) in 1 mL of D_2O and then irradiated under purple LEDs (λ > 395 nm, 6 W) with magnetic stirring in air for 5 h at r.t. Then the reaction mixture was extracted with CH_2Cl_2 without further purification. [b] Yields were obtained from ^{1}H NMR integration based on 1,3,5-trimethoxybenzene as the internal standard (0.003 mmol L^{-1}) (Fig. S25–S37†). [c] Ph_4BNa (0.002 mmol, 2 equiv.) was added as an inhibitor. [d] Under a N_2 atmosphere. [e] Replacing cage **1** with $L^1{\cdot}BF_4$. [f] Replacing cage **1** with $(tmen)Pd(NO_3)_2$. [g] Under darkness.

Open Access Article. Published on 15 May 2023. Downloaded on 8/6/2025 5:20:31 AM.
This article is licensed under a Creative Commons Attribution 3.0 Unported Licence.

experiments (Table 1, entries 3, 6 and Fig. S42, S43†) showed that the photooxidation/Knoevenagel condensation of **3a** did not proceed without air or under darkness. Under the same reaction conditions, cage components, L^1 and $(tmen)Pd(NO_3)_2$, also did not catalyze the reaction, while cage **2**, without the pyridine active sites, gave a much lower yield (66%) (Table 1, entries 4, 5, 7 and Fig. S40, S41, S47†).

We also monitored the two catalytic reaction processes under other conditions (15 equiv. of **3a**). The results (Fig. S48†) showed that the yield of **4a** catalyzed by cage **1** rapidly reached 71% at 2 h and finally became 97% after 5 h, while the yield catalyzed by cage **2** was only 22% at 2 h and reached 86% after 10 h in comparison. The reaction rates were found to be nearly linearly dependent on the substrate concentration in our system, as the reaction at a concentration of 30 mM of **3a** was *ca.* 1.9 times faster than that at a concentration of 15 mM (Fig. S50†).

A wide substrate scope was noticed for this reaction, as a series of electron-rich and electron-deficient benzyl alcohols (Table 1 and Fig. S27–S37†) could be efficiently converted to the corresponding α,β-unsaturated dinitriles in moderate to good yields (Table 1, entries 8–14), where electron-rich alcohols often show higher yields than electron-deficient ones. While two naphthalenyl alcohols could be used for this reaction, no reaction of the bulky pyren-1-ylmethanol (**3k**) was observed (Table 1, entry 17). The ^{1}H NMR spectrum showed that **3k** cannot be encapsulated by cage **1** due to its bulky size (Fig. S37†). Meanwhile, in inhibition experiments with sodium tetraphenylborate (Ph_4B^-, a strong binding guest of cage **1**), the formation of **4a** was significantly inhibited, resulting in a much lower yield (27%) (Fig. S38 and S39†). This indicated that hydrophobic encapsulation of the substrates is essential for the reaction. The turnover number (TON) of cage **1** was determined by lowering the loading of cage **1** to 0.67 mol% (150 equiv. of **3a** in total). A TON of 134 in 40 h was achieved, offering 89% isolated yield of **4a** (Fig. S44 and Table S1†). Clean and unchanged ^{1}H NMR signals after the reaction suggest the structural robustness of cage **1**. A slight decrease of the cage's concentration was noticed, which we infer was due to co-precipitation of the cage with the insoluble products (Fig. S45†).

To elucidate the reactive oxygen species involved during the reaction, 10 equiv. of *t*-butyl alcohol ($^{\bullet}$OH capturing agent), NaN_3 ($^1O_2$ quencher) or benzoquinone ($O_2^{\bullet-}$ capturing agent) was added to the reaction mixture. While *t*-butyl showed a negligible effect on the reaction (Fig. S61†), the presence of NaN_3 and benzoquinone significantly inhibited the photooxidation–Knoevenagel condensation of **3a**, with only 8% and 18% yields detected, respectively (Fig. S62 and S63†). These results indicate that $^1O_2$ and $O_2^{\bullet-}$ are the oxidizing species in the photooxidation reaction, and $O_2^{\bullet-}$ should be dominant in the electron transfer process.

Mechanistic discussion

We rationalize the mechanism for the enhanced one-pot photooxidation/Knoevenagel condensation reaction by cage **1** based on the following facts:

(i) The substrate was encapsulated by cage **1** through a hydrophobic effect and π–π stacking interactions. The ^{1}H NMR titration spectra of **1** with representative **3a** and 1-naphthalenemethanol (**3i**) showed that the guest signals were clearly downfield-shifted, and cage **1** exhibits a fast-exchange binding mode for **3i** with the apparent binding constant determined to be 672 M^{-1} (Fig. S55 and S56†) by Hill function fitting. The apparent binding constant for the reaction intermediate 4-bromobenzaldehyde was determined to be 223 M^{-1}, which is lower than K_a (273 M^{-1}) for **3a** (Fig. S51–S54†). However, cage **1**

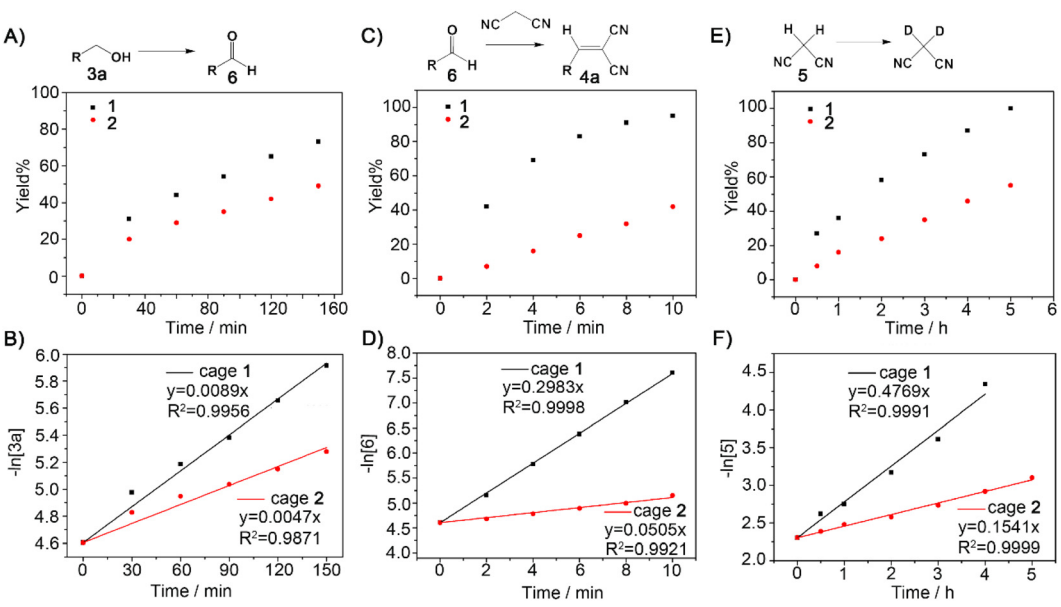

Fig. 5 Yields and the corresponding first-order kinetic plots for the cage (**1** and **2**) catalysed photooxidation reaction of **3a** (A and B), the Knoevenagel condensation of 4-bromobenzaldehyde **6** with malononitrile (C and D) and the deuteration of malononitrile **5** (E and F) in D_2O.

This journal is © The Royal Society of Chemistry 2023

Open Access Article. Published on 15 May 2023. Downloaded on 8/6/2025 5:20:31 AM. This article is licensed under a Creative Commons Attribution 3.0 Unported Licence.

showed a stronger binding ability towards 1-naphthaldehyde, with K_a = 881 M^{-1} (Fig. S57 and S58†).

(ii) Upon light irradiation, the electron-deficient pyridinium ligands on cage **1** can receive an electron from the reductive alcohol to form the free radical state. The UV-vis absorption spectra of cage **1** after addition of **3a** showed a new charge-transfer band tailing in the range of 300–400 nm, which was enhanced after photoirradiation (Fig. S21 and S22†). Electron spin resonance spectroscopy (ESR) confirmed the generation of the radicals, with the emergence of ESR signals (g = 2.0065) after irradiation of the solution containing cage **1** and **3i** (Fig. S24†). The excited state of the host–guest complexes leads to the generation of reactive oxygen species ($^1O_2$ and $O_2^{\bullet-}$) by energy transfer or electron transfer, which facilitate the photocatalytic oxidation of benzyl alcohols. It is worth noting that the photo-oxidation rate of **3a** is faster with cage **1** as the catalyst compared to that of cage **2**, under the same reaction conditions (Fig. 5A and B).

(iii) Malononitrile became deprotonated to give the carbanion nucleophile due to the cationic nature of the cages and the existence of Brønsted-base sites. The H/D exchange reaction of malononitrile catalyzed by cage **1** in D_2O was completed in 100% yield over a period of 5 h. A much faster deuteration rate is observed for cage **1** (k_1 = 0.48 h^{-1}) in comparison with cage **2** (k_1 = 0.15 h^{-1}), verifying the effective C–H activation of malononitrile by the Brønsted-base centers (Fig. 5E and F).

(iv) The carbanion immediately attacks the aromatic aldehyde substrate to form the β-hydroxy intermediate, which is subsequently rearranged and dehydrated to the final product. Kinetic studies on a model Knoevenagel condensation between 4-bromobenzaldehyde (**6**) and malononitrile shows that this reaction catalyzed by cage **1** is *ca.* 6 times faster than that catalyzed by cage **2** (Fig. 5C and D).

(v) NMR titrations by adding **4a** into cage **1** confirmed that the condensation product cannot be encapsulated by cage **1** (Fig. S60†). This is consistent with the fact that the product settled down during the reaction, which facilitated the turnover of the catalytic cycle.

Conclusions

In conclusion, we have constructed a new Brønsted-base functionalized molecular cage that exhibits excellent catalytic performance in the one-pot sequential photooxidation/Knoevenagel condensation reaction, featuring high reactivity, high TON and broad substrate scope. Our results demonstrate that new catalytic functions can be activated by introducing active sites that cooperate with the confinement cavities of the host, offering new insight into the construction of functionalized nanoreactors.

Experimental section

General

Unless otherwise stated, all chemicals and solvents were purchased from commercial companies and used without further purification. Deuterated solvents were purchased from Admas, Sigma-Aldrich and J&K Scientific. 1D and 2D NMR spectra were measured on a Bruker Biospin Avance III (400 MHz) or a JEOL ECZ600S (600 MHz) spectrometer. The NMR chemical shifts (δ) are reported in ppm (parts per million) with respect to the solvent signal that originated due to incomplete deuteration (δ = 4.79 for D_2O, δ = 2.50 for DMSO-d_6, δ = 7.26 for $CDCl_3$ in ^{1}H NMR). UV-Vis absorption spectra were recorded on a UV-2700 UV-Visible spectrophotometer from SHIMADZU Corporation. ESI-TOF-MS spectra were recorded on an Impact II UHR-TOF mass spectrometer from Bruker or LC-QTOF-MS (G6520B). Data analyses were conducted using the Bruker Data Analysis software (Version 4.3) and simulations were performed using the Bruker Isotope Pattern software or Thermo Xcalibur Qual Browser software (Thermo Foundation 2.0). Electrochemical analysis was performed on a CHI 604E analyzer. All cyclic voltammetry (CV) experiments were carried out in argon-purged solutions of DMSO at room temperature. The purple LED light sources used for all the photoreactions in this research were from Wuhan Geo Instruments Science & Technology Co., Ltd (China) (λ > 395 nm; 1 W for every lamp bead; every Schlenk tube was irradiated using 6 lamp beads from the side).

Synthesis of ligands L^1 and L^2

2,4,6-Tris(4-pyridyl)-1,3,5-triazine (420 mg, 1.346 mmol) was added to dry dimethylformamide (120 mL) under a nitrogen atmosphere and the suspension was stirred at 120 °C until it became clear. The solution was treated drop-wise with 2,6-bis(bromomethyl)pyridine (143 mg, 0.540 mmol) dissolved in a small amount of DMF and then maintained at 115 °C for 5 h, affording a reddish-brown clear solution. The solution was cooled to room temperature and placed in a refrigerator below 0 °C overnight, affording a reddish-brown turbid liquid. The turbid liquid was filtered to remove excess TPT, giving a reddish-brown clear solution. The solvent was removed by reduced pressure distillation to give a yellowish-green precipitate. Then, the precipitate was collected by filtration and the filter cake was dissolved in hot water to remove excess TPT, followed by the addition of an excess of sodium tetrafluoroborate ($NaBF_4$). A purple solid of pure L^1 $(BF_4)_2$ (M = 903.41 g mol^{-1}, 228 mg, yield 46.7%) was collected by filtration. ^{1}H NMR (600 MHz, DMSO-d_6) δ 9.12 (d, J = 6.8 Hz, 4H), 9.10 (d, J = 7.0 Hz, 4H), 8.69 (d, J = 6.0 Hz, 8H), 8.25 (d, J = 6.0 Hz, 8H), 8.18 (t, J = 7.8 Hz, 1H), 7.76 (d, J = 7.8 Hz, 2H), 6.20 (s, 4H). ^{13}C NMR (101 MHz, DMSO) δ 171.3 (s), 168.0 (s), 152.9 (s), 151.2 (s), 149.5 (s), 148.0 (s), 140.9 (s), 126.5 (s), 122.5 (s), 122.2 (s), 65.4 (s), 63.6 (s). ESI-TOF-MS: m/z Calcd for $[L(BF_4)]^{1+}$ 816.2856 found 816.2843.

L^2 was synthesized by a similar procedure, starting from 1,3-bis(bromomethyl)benzene (102 mg, 0.385 mmol). Pure L^2 $(BF_4)_2$ was obtained in a yield of 10.4% (M = 902.42 g mol^{-1}, 36 mg). ^{1}H NMR (600 MHz, DMSO-d_6) δ 9.45 (d, J = 6.2 Hz, 4H), 9.39 (d, J = 6.2 Hz, 4H), 8.97 (d, J = 6.0 Hz, 8H), 8.67 (d, J = 6.0 Hz, 8H), 7.63–7.61 (m, 4H), 6.07 (s, 4H). ^{13}C NMR (101 MHz, DMSO-d_6) δ 171.7 (s), 165.7 (s), 151.7 (s), 147.0 (s), 142.6 (s), 142.1 (s), 134.8

Open Access Article. Published on 15 May 2023. Downloaded on 8/6/2025 5:20:31 AM. This article is licensed under a Creative Commons Attribution 3.0 Unported Licence.

(s), 130.1 (s), 127.7 (s), 122.8 (s), 75.8 (s), 66.8 (s), 63.7 (s). ESI-TOF-MS: *m*/*z* Calcd for $[L(BF_4)]^{1+}$ 815.2904 found 815.2895.

Synthesis of cage 1 ($Pd_4L^1{}_2$)

Ligand L^1 (BF_4 salt, 8.03 mg, 8.89 μmol) was treated with (tmen)$Pd(NO_3)_2$ (5.54 mg, 16.00 μmol) in D_2O (4 mL) at 50 °C for 15 min. The suspension progressively dissolved to generate a homogeneous light-orange solution. ^{1}H NMR confirmed the quantitative formation of $Pd_4L^1{}_2{\cdot}(BF_4)_4(NO_3)_8$ (cage **1**, M = 3193 g mol^{-1}).^{1}H NMR (400 MHz, D_2O) δ 9.35 (d, J = 5.8 Hz, 8H), 9.28 (d, J = 5.8 Hz, 8H), 9.09 (d, J = 6.6 Hz, 8H), 9.04 (d, J = 6.4 Hz, 8H), 8.76 (t, J = 6.6 Hz, 16H), 8.24 (t, J = 7.8 Hz, 2H), 7.95 (d, J = 7.8 Hz, 4H), 6.10 (s, 8H), 3.16 (s, 16H), 2.74 (d, J = 7.6 Hz, 48H). ^{13}C NMR (101 MHz, D_2O) δ 169.6 (s), 168.7 (s), 151.9 (s), 151.2 (s), 150.2 (s), 145.9 (s), 145.3 (s), 126.7 (s), 126.6 (s), 126.0 (s), 64.8 (s), 62.6 (s), 50.3 (s), 50.1 (d).

$Pd_4L^1{}_2{\cdot}(PF_6)_{12}$ was prepared by treating $Pd_4L^1{}_2{\cdot}(BF_4)_4(NO_3)_8$ with excess ammonium hexafluorophosphate in an aqueous medium for electrospray ionization mass spectra (ESI-MS) measurement. ESI-TOF-MS: *m*/*z* Calcd for $[Pd_4L^1{}_2{\cdot}(PF_6)_8]^{4+}$ 877.3555 found 877.3541.

Synthesis of cage 2 ($Pd_4L^2{}_2$)

Ligand L^2 (BF_4 salt, 8.02 mg, 8.89 μmol) was treated with (tmen)$Pd(NO_3)_2$ (5.54 mg, 16.00 μmol) in D_2O (4 mL) at 70 °C for 30 min. The suspension progressively dissolved to generate a homogeneous light-yellow solution.^{1}H NMR confirmed the quantitative formation of $Pd_4L^2{}_2{\cdot}(BF_4)_4(NO_3)_8$ (cage **2**, M = 3191 g mol^{-1}). ^{1}H NMR (600 MHz, D_2O) δ 9.33 (d, J = 6.0 Hz, 8H), 9.26 (d, J = 6.0 Hz, 8H), 9.13 (d, J = 6.8 Hz, 8H), 9.02 (d, J = 6.8 Hz, 8H), 8.76 (d, J = 7.2 Hz, 8H), 8.74 (d, J = 6.0 Hz, 8H), 7.96 (d, J = 9.6 Hz, 2H), 7.85–7.80 (m, 6H), 5.93 (s, 8H), 3.14 (s, 16H), 2.70 (d, J = 15.2 Hz, 48H). ^{13}C NMR (101 MHz, D_2O) δ 169.5 (s), 168.6 (s), 151.9 (s), 149.9 (s), 145.3 (s), 133.0 (s), 132.8 (s), 126.9 (s), 126.0 (s), 64.3 (s), 62.8 (s), 62.6 (s), 50.3 (s), 50.1 (s).

$Pd_4L^2{}_2{\cdot}(PF_6)_4$ was prepared by treating $Pd_4L^2{}_2{\cdot}(BF_4)_4(NO_3)_8$ with excess ammonium hexafluorophosphate in an aqueous medium for electrospray ionization mass spectra (ESI-MS) measurement. ESI-TOF-MS: *m*/*z* Calcd for $[Pd_4L^2{}_2{\cdot}(PF_6)_8]^{4+}$ 876.8579 found 876.8575.

Author contributions

The manuscript was written through contributions of all authors. All authors have given approval to the final version of the manuscript.

Conflicts of interest

There are no conflicts to declare.

Acknowledgements

This work was supported by the National Key Research and Development Program of China (Grants 2021YFA1500400 and 2022YFA1503300), the National Natural Science Foundation of China (Grants 22171264, 22171262 and 21825107), and the Natural Science Foundation of Fujian Province (Grants 2021J01516 and 2021J02016).

References

1 C. B. Anfinsen, *Science*, 1973, **181**, 223.
2 R. Breslow and S. D. Dong, *Chem. Rev.*, 1998, 1997.
3 Y. Fang, J. A. Powell, E. Li, Q. Wang, Z. Perry, A. Kirchon, X. Yang, Z. Xiao, C. Zhu, L. Zhang, F. Huang and H. C. Zhou, *Chem. Soc. Rev.*, 2019, **48**, 4707.
4 X. Z. Li, C. B. Tian and Q. F. Sun, *Chem. Rev.*, 2022, **122**, 6374.
5 W. Liu and J. F. Stoddart, *Chem*, 2021, **7**, 919.
6 J. Piera and J.-E. Bäckvall, *Angew. Chem.*, 2008, **120**, 3558.
7 J. Meeuwissen and J. N. Reek, *Nat. Chem.*, 2010, **2**, 615.
8 C. J. Brown, F. D. Toste, R. G. Bergman and K. N. Raymond, *Chem. Rev.*, 2015, **115**, 3012.
9 S. C. Li, L. X. Cai, M. Hong, Q. Chen and Q. F. Sun, *Angew. Chem., Int. Ed.*, 2022, **61**, e202204732.
10 C. Ngai, C. M. Sanchez-Marsetti, W. H. Harman and R. J. Hooley, *Angew. Chem., Int. Ed.*, 2020, **59**, 23505.
11 M. J. Wiester, P. A. Ulmann and C. A. Mirkin, *Angew. Chem., Int. Ed.*, 2011, **50**, 114.
12 R. Saha, B. Mondal and P. S. Mukherjee, *Chem. Rev.*, 2022, **122**, 12244.
13 Z. Dong, Q. Luo and J. Liu, *Chem. Soc. Rev.*, 2012, **41**, 7890.
14 T. S. Koblenz, J. Wassenaar and J. N. Reek, *Chem. Soc. Rev.*, 2008, **37**, 247.
15 M. Raynal, P. Ballester, A. Vidal-Ferran and P. W. van Leeuwen, *Chem. Soc. Rev.*, 2014, **43**, 1734.
16 D. A. Roberts, B. S. Pilgrim, J. D. Cooper, T. K. Ronson, S. Zarra and J. R. Nitschke, *J. Am. Chem. Soc.*, 2015, **137**, 10068.
17 Y. Ueda, H. Ito, D. Fujita and M. Fujita, *J. Am. Chem. Soc.*, 2017, **139**, 6090.
18 D. Fujita, Y. Ueda, S. Sato, N. Mizuno, T. Kumasaka and M. Fujita, *Nature*, 2016, **540**, 563.
19 L. R. MacGillivray and J. L. Atwood, *Nature*, 1997, **389**, 469.
20 B. Olenyuk, J. A. Whiteford, A. Fechtenkötter and P. J. Stang, *Nature*, 1999, **398**, 796.
21 D. M. Kaphan, M. D. Levin, R. G. Bergman, K. N. Raymond and F. D. Toste, *Science*, 2015, **350**, 1235.
22 K. Li, K. Wu, Y. L. Lu, J. Guo, P. Hu and C. Y. Su, *Angew. Chem., Int. Ed.*, 2022, **61**, e202114070.
23 H. Jiang, W. Zhang, X. Kang, Z. Cao, X. Chen, Y. Liu and Y. Cui, *J. Am. Chem. Soc.*, 2020, **142**, 9642.
24 T. Hong, Z. Zhang, Y. Sun, J. J. Tao, J. D. Tang, C. Xie, M. Wang, F. Chen, S. S. Xie, S. Li and P. J. Stang, *J. Am. Chem. Soc.*, 2020, **142**, 10244.

This journal is © The Royal Society of Chemistry 2023

Open Access Article. Published on 15 May 2023. Downloaded on 8/6/2025 5:20:31 AM.
This article is licensed under a Creative Commons Attribution 3.0 Unported Licence.

25 J. Guo, Y. W. Xu, K. Li, L. M. Xiao, S. Chen, K. Wu, X. D. Chen, Y. Z. Fan, J. M. Liu and C. Y. Su, *Angew. Chem., Int. Ed.*, 2017, **56**, 3852.
26 J. Wei, L. Zhao, C. He, S. Zheng, J. N. H. Reek and C. Duan, *J. Am. Chem. Soc.*, 2019, **141**, 12707.
27 A. G. Salles Jr., S. Zarra, R. M. Turner and J. R. Nitschke, *J. Am. Chem. Soc.*, 2013, **135**, 19143.
28 J. Wei, L. Zhao, Y. Zhang, G. Han, C. He, C. Wang and C. Duan, *J. Am. Chem. Soc.*, 2023, **145**, 6719.
29 P. J. Parsons, C. S. Penkett and A. J. Shell, *Chem. Rev.*, 1996, **96**, 195.
30 K. Li, K. Wu, Y.-Z. Fan, J. Guo, Y.-L. Lu, Y.-F. Wang, G. Maurin and C.-Y. Su, *Natl. Sci. Rev.*, 2021, **9**, 155.
31 F.-F. Zhu, L.-J. Chen, S. Chen, G.-Y. Wu, W.-L. Jiang, J.-C. Shen, Y. Qin, L. Xu and H.-B. Yang, *Chem*, 2020, **6**, 2395.
32 J. Jiao, Z. Li, Z. Qiao, X. Li, Y. Liu, J. Dong, J. Jiang and Y. Cui, *Nat. Commun.*, 2018, **9**, 4423.
33 Y.-B. Huang, J. Liang, X.-S. Wang and R. Cao, *Chem. Soc. Rev.*, 2017, **46**, 126.
34 L. R. Holloway, P. M. Bogie, Y. Lyon, C. Ngai, T. F. Miller, R. R. Julian and R. J. Hooley, *J. Am. Chem. Soc.*, 2018, **140**, 8078.
35 D. N. Yan, L. X. Cai, P. M. Cheng, S. J. Hu, L. P. Zhou and Q. F. Sun, *J. Am. Chem. Soc.*, 2021, **143**, 16087.
36 S.-C. Li, L.-X. Cai, L.-P. Zhou, F. Guo and Q.-F. Sun, *Sci. China: Chem.*, 2019, **62**, 713.
37 L. X. Cai, S. C. Li, D. N. Yan, L. P. Zhou, F. Guo and Q. F. Sun, *J. Am. Chem. Soc.*, 2018, **140**, 4869.
38 N. R. Voss and M. Gerstein, *Nucleic Acids Res.*, 2010, **38**, W555.